Desalination and Water Treatment
www.deswater.com

doi: 10.5004/dwt.2023.29135

281 (2023) 234–248
January

Enhanced adsorption of ceftriaxone antibiotics from water by mesoporous copper oxide nanosphere

Amnah Mohammed Alsuhaibani[a], Moamen S. Refat[b], Abdel Majid A. Adam[b], Mohamed G. El-Desouky[c,*], Ashraf A. El-Bindary[d]

[a]*Department of Physical Sport Science, College of Education, Princess Nourah bint Abdulrahman University, P.O. Box: 84428, Riyadh 11671, Saudi Arabia, email: amalsuhaibani@pnu.edu.sa*
[b]*Department of Chemistry, College of Science, Taif University, P.O. Box: 11099, Taif 21944, Saudi Arabia, emails: moamen@tu.edu.sa (M.S. Refat), majidadam@tu.edu.sa (A.M.A. Adam)*
[c]*Egyptian Propylene and Polypropylene Company, Port Said 42511, Egypt, email: ch.moh.gamal@gmail.com*
[d]*Chemistry Department, Faculty of Science, Damietta University, Damietta 34517, Egypt, email: abindary@yahoo.com*

Received 23 July 2022; Accepted 17 November 2022

ABSTRACT

This work investigated the removal of antibiotic ceftriaxone (CEF) from wastewater using mesoporous copper oxide nanosphere as synthesized resulted from calcination organometallic chelate, and characterized by X-ray diffraction, Fourier-transform infrared spectroscopy, energy-dispersive X-ray spectroscopy, including the Brunauer–Emmett–Teller variable surface area, which was 78.83 m^2/g. Scanning electron microscopy got accustomed to quantify the changes on the surface. CEF was accomplished at pH 7, which is the ideal adsorption setting. The thermodynamic analysis was done at a variety of temperatures between 25°C and 45°C. The thermodynamic parameters that were obtained highlight a reduction in the adsorption process' endothermic, random, and spontaneous. The kinetic studies demonstrated that more than one mechanism would affect the diffusion of ceftriaxone from the solution into the copper oxide and that the pseudo-second-order model might provide a better fit of the test findings. According to the isotherm investigations, the Langmuir model, having the highest adsorption capacity of 127 mg/g, provided the best fit to the isotherm curve. Adsorption's activation energy was also found to be 14.43 kJ/mol, demonstrating that chemisorption process. It was calculated that the adsorption mechanism was endothermic as the negativity of $\Delta G°$ was increase with increase the temperature and spontaneous. Also determine thermodynamic parameter $\Delta G°$, $\Delta H°$ and $\Delta S°$. A quick and efficient method of purifying water was found to be the mesoporous copper oxide nanosphere adsorbent. Copper oxide nanosphere material has shown promise in the process of removing CEF from aqueous solution. Surprisingly, the synthesized adsorbent displayed a remarkable recyclability of >91.2% up to the sixth cycle. According to the findings, CuO can be employed as a ceftriaxone adsorbent for aqueous mediums at a reasonable cost. On other hand, it was simple to remove the CuO nanosphere from the solution and regenerate it with washing.

Keywords: Adsorption; Kinetics; Isotherm; Thermodynamics; Ceftriaxone

* Corresponding author.

1. Introduction

The CuO nanosphere may be readily removed from the solution and cleaned to regenerate it [1–3]. These sorts of environmental contaminants generate health risks resulting in the release of APIs (active pharmaceutical ingredients), enhanced microbial resistance, an increase in the cytotoxic potential of chemical substances and metabolites, a slowing in the oxidation of nitrite and methanogenesis [4,5]. Ceftriaxone, like other third-generation cephalosporins, is among the most significant antibiotics used to treat diseases and displays a wide range of gram-positive and gram-negative bacterial activities. Antibiotics can accumulate in soils and sediments, which can have a negative impact on the ecosystem's ability to operate naturally and slow down the normal degradation of contaminants [6,7]. Additionally, drinking water sources can allow antibiotic-resistant genes to enter, leading to the development of illnesses. Due to their constant entry into the surroundings, antibiotics are stable and lipophilic and can linger there for a very long period. Both high and low concentrations of antibiotics are harmful [8,9].

Additionally, bacterial resistance may be accelerated by the persistence and accumulation of antibiotics in water, that is thought to be one of the primary causes of environmental pollution. Some antibiotics have been labelled as hazardous and carcinogenic due to their high toxicity and poor biodegradability [10,11]. Traditional wastewater treatment techniques, such as activated sludge, are insufficient for completely eliminating active pharmaceutical ingredients and other wastewater elements. Therefore, using current methods, only 60%–90% of antibiotics can be extracted [12,13]. Owing to the adsorption method's straightforward construction, convenience of use, and relatively simple regeneration, a variety of antibiotics pollutants were removed from the environment utilizing it [14,15].

Cephalosporins are a class of -lactam antibiotics, as Edward Abraham and colleagues discovered in 1948 [16,17]. CEF, a third-generation antibiotic from the family of cephalosporins, is used to eradicate organisms that typically exhibit antibiotic resistance. Synthetic fluoroquinolone compounds have earned a reputation as the most popular antibiotics for curing bacterial infections that affect both humans and animals [18–22].

Numerous scientific studies and publications revealed that the overpopulation issue, as well as the development in agricultural and animal husbandry activities, has caused a sharp rise in the production of pharmaceuticals globally, particularly antibiotics. Public health issues brought on by pathogens' antibiotic resistance are still another significant factor that certain research have mentioned [23,24]. As a result, it is necessary to lengthen the time that patients are exposed to and the doses of antibiotics they take throughout therapy, which necessitates an increase in the rate at which new medicines are produced [25]. The average annual production rate of medical chemicals during the past 10 y has been between 100,000 and 200,000 tonnes. In actuality, the majority of the substances were antibiotics, which were employed as drugs to treat humans, animals, and fowl as well as an antibacterial infection agent. Indeed, considerable amounts of antibiotic residuals were found in the soil and aquatic ecosystem. The findings of current research on the potential health effects of drinking water tainted with pharmaceuticals are alarming. Ceftriaxone (CEF), a broad-spectrum antibacterial drug that is a member of the so-called "fluoroquinolones class", has been used extensively to treat various infectious diseases. This antibiotic's chemical makeup includes fluorine atoms, which gives it the property of being extremely stable (having a low degradation rate) [26].

Furthermore, CEF is highly soluble in water (1.35 mg/mL). Many tests of surface water and municipal wastewater from various sites across the world contained CEF residues with concentrations greater than 1 g/L. While its concentration might reach 150 g/L in the hospital and pharmaceutical industry's liquid waste. In actuality, antibiotic residuals result from their adequate non-metabolism in

Fig. 1. Adsorption mechanism for CEF is depicted schematically using CuO.

both human and animal bodies, and they can therefore be eliminated into municipal industrial effluent through urine and faeces. Other sources of antibiotic residuals include distributing out-of-date medications with liquid pharmaceutical waste, a small amount of veterinary and agricultural wastewater as well as lab and research untreated sewage. Environmental scientists caution that antibiotic residues, particularly those found in water sources used for drinking, can have harmful impacts on people, animals, and other living things since they include poisonous and cancerous substances [27]. Reduced fertility, breast and prostate cancers, prenatal mutations, DNA damage, and damaged lymphocytes are a few impacts of improper antibiotic use that have been observed in humans [28].

To remove pollutants containing pharmaceutical substances, a variety of techniques, there have been uses for physical, chemical, biological, and even a combination of these processes. Nevertheless, it was discovered that several of the suggested treatment options have a number of drawbacks in terms of effectiveness and cost. Owing to its capacity to effectively remove a number of contaminants from wastewater in an easy and affordable manner, adsorption is a widely desired therapeutic approach. Additionally, this treatment approach does not generate contaminants while it is being used, in contrast to other procedures like degradation or chemical oxidation [26,29].

In this research, we investigated how well CuO nanospheres removed ceftriaxone (CEF) from aqueous solution. Waste management to eliminate CEF has become crucial for the environment as a result of CEF. Additionally, because of their aromatic structure, they are more stable and more resistant to degradation. Variety of approaches were recommended for systematic material characterization of the CuO nanosphere as it had been produced. Among the experimental variables looked at were the adsorbent dose, initial adsorbate concentration, solution, contact time, pH, and temperature. The experimental equilibrium adsorption data were examined using both the kinetic and isotherm models. The thermodynamic parameters were assessed in order to explain the operation's process.

2. Materials and methods

2.1. Materials

The ligand and its complex was prepared previously and illustrated on their synthesis and characterization at supplementary material [30].

2.2. Preparation of CuO nanosphere

The CuO was obtained by calcination of $[CuCl(OH_2)]\cdot 2H_2O$ chelate at temperatures of 450°C, 550°C, and 650°C for 4 h. This method produces CuO nanosphere quickly and easily, without utilizing costly, toxic chemicals or sophisticated machinery [31].

2.3. Characterization of CuO

The instrument and method used in characterization illustrated in detail at (Supplementary material).

2.4. Preparation of adsorbate

Ceftriaxone with concentration (1×10^{-3} mol/L) of was prepared using bidi stilled water during the preparation of the stock solutions and during the experimental study.

2.5. Adsorption experiments

With 0.02–0.1 g of CuO as the adsorbent, the batch equilibrium technique was used for the CEF adsorption investigations with a 25 mL CEF solution (2.51×10^{-3} mol/L) 100 min passed with pHs of the solution ranging from 1 to 12 after HCl or NaOH (1 M) adjustments. It was determined what pH was best and all adsorption processes followed it. To determine if the equilibrium in adsorption and ideal CEF removal could be achieved, surveys were performed over a variety of time intervals. Using a Whatman (number 40) filter paper used for the filtering of the solution from any contaminants, the extract was first filtered before being submitted for quantification (Fig. 1). The concentration of CEF solution was determined at UV-maximum wavelength, (λ_{max}) at 241 nm. In order to get isotherms at various temperatures (25°C–50°C), CEF adsorption isotherms were also conducted utilizing a thermal shaker. Calibration curves for CEF were developed to link concentrations to different absorbances [32].

The (%) removal of CEF and the adsorption capacity were estimated using Eqs. (1) and (2), respectively:

$$\%R = \frac{\left(C_0 - C_t\right)}{C_0} \times 100 \tag{1}$$

where C_0 is the CEF solution's initial concentration, C_e is the CEF equilibrium time concentration.

Using the weight balance equation, the adsorption efficiency was determined [Eq. (2)] (q_e, mmol/g):

$$q_e = \frac{\left(C_0 - C_e\right)V}{m} \tag{2}$$

where m (g) is the CuO adsorbent mass and V (L) volume of the CEF solution.

3. Results and discussion

3.1. Characterization of CuO

3.1.1. X-ray diffraction patterns

Fig. 2 displays the CuO X-ray diffraction (XRD) data at various temperatures. CuO formed into a tetragonal structure with lattice constants, as evidenced by the detected diffraction peaks linked to well-crystallized CuO where, a = 6.98, b = 11.14 and c = 5.112 Å, α = 90.0°, β = 90° and γ = 108.94°. That indicate the existence of CuO in monoclinic from. The interplanar spacing (d_{hkl}) and Miller indices (hkl) for CuO are recorded in Table 1 (Space group P21/c, also, formation energy/atom was –4.5 eV and energy above hull/atom 0.39 eV).

No extra peaks due to contamination were detected, this considered great evidence of the high purity of the prepared

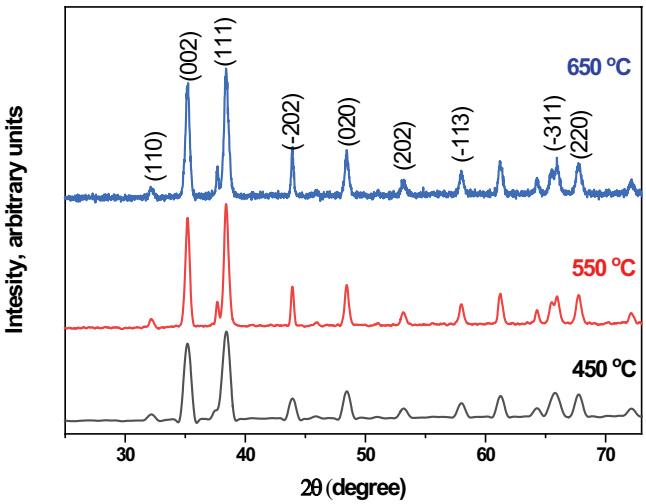

Fig. 2. XRD of CuO nanosphere.

Table 1
Crystallographic of CuO

$2\theta_{Obs.}$ (°)	$2\theta_{Calc.}$ (°)	$d_{hkl(Obs.)}$ (Å)	$d_{hkl(Calc.)}$ (Å)	(*hkl*)
32.204	32.16	2.7796	2.7833	040
36.187	36.142	2.4822	2.4852	–112
38.423	38.447	2.3427	2.3414	–202
61.261	61.216	1.5131	1.514	152
64.299	64.323	1.4487	1.4482	113
65.817	65.812	1.4189	1.419	–440
67.766	67.789	1.3828	1.3824	421
72.167	72.215	1.3089	1.3082	–371
77.472	77.412	1.232	1.2328	460
79.697	79.733	1.2031	1.2026	281

CuO. Also, the identical XRD patterns of the CuO samples at various temperatures may be seen. The crystal planes (110), (002), (111), (–202), (020), (–113), (–311) and (220) of bulk CuO can be easily indexed at 2θ = 32.24°, 34.89°, 63.37°, 48.65°, 75.31°, 63.4°, 68.5° and 69.66°, respectively. By using Scherrer formula Eq. (3) the crystallite size (*D*, Å) of the ZnO nanosphere was calculated [33].

$$D = \frac{K\lambda}{\beta \mathrm{Cos}\theta B} \tag{3}$$

At temperatures of 450°C, 550°C, and 650°C, respectively, the CuO crystallite size measured from the high-intensity (101) peak was 22, 29, 32, and 33.35 nm. It is clear that when temperature rises, the average grain size rises while the specific surface area decreases. The greater amount of CuO particle accumulation provides an explanation for these findings [34].

3.1.2. Brunauer–Emmett–Teller surface area

Because the size and number of pores can significantly affect a substance's properties and its capacity for handling,

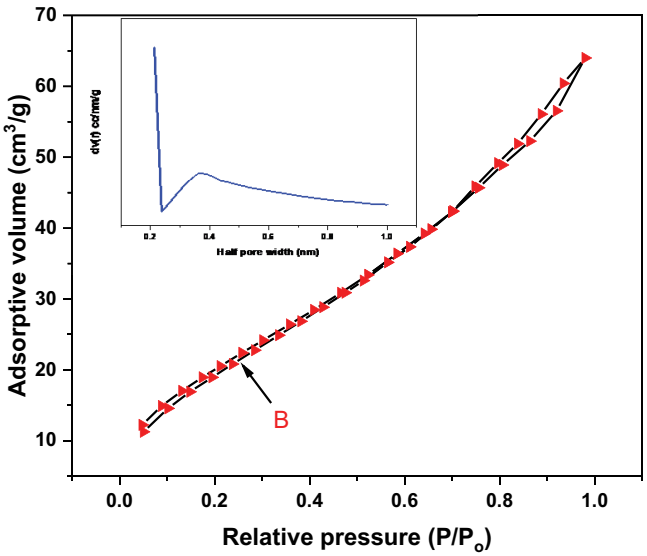

Fig. 3. For N_2, the CuO adsorption/desorption isotherm occurs at 450°C.

in a porous material, determining the effective surface area of the holes is extremely important. This is commonly accomplished by measurement the material's Brunauer–Emmett–Teller (BET) area of contact. Surface interactions occur when a gas interacts with a substance's outer surface. BET examinations are based on the probability that a gas would get poorly attached to a substance's surface and an adsorption isotherm that is dependent on physisorption. Since physisorption is reversible, a gas can swiftly adsorb and desorb to a substance's surfaces.

The adsorption isotherm, which measures volume, is the result of changing pressures of gas being absorbed while maintaining a constant temperature. Since liquid nitrogen is used to keep the temperature stable, it is around 77 K. The complete adsorption isotherm graph can be produced by plotting the amount of gas adsorbed against the relative pressures. Curves shape of the plot shows the Type II of porosity existing at substance (Fig. 3) as well as the sort of pores in the substance. Monolayer-multilayer adsorption without restriction is represented by the Type II isotherm. Point B, which marks the start of the isotherm's nearly linear middle part, is frequently chosen. The presence of a hysteresis loop is shown by type I adsorption isotherms for CuO. The two branches are nearly parallel and virtually vertical in the former throughout a sizable range of gas uptake, whereas they are nearly horizontal and parallel in the latter over a broad range of p/p^0. As a result, Type HI is frequently linked to porous materials that are known from other sources to display limited distributions in pore size because they are composed of aggregates or compacts of roughly uniform spheres organized in a fairly regular fashion. Adsorption effectiveness of the sample calcined at 450°C is higher in our case. Which has a lower crystallite1 size and a larger specific surface area than the others (78.38 m^2/g), pore size 2.53 nm which according to IUPAC it will be classified as mesoporous [35].

3.1.3. Scanning electron microscopy analysis

Scanning electron microscopy (SEM) was used to investigate the surface characteristics of CuO nanosphere (Fig. 4) shows the homogeneous growth of CuO. The cultivated nanostructures are in the form of nanosphere that were interlinked and created pores and fissures, resulting in vast surface areas for rapid dye dispersion on metal oxide surfaces, SEM photos at greater microscopy demonstrate this. CuO nanosphere having a diameter about 46 nm were approved by SEM examination [36,37].

3.1.4. Energy-dispersive X-ray spectroscopy

Owing to its atoms, each material will have its X-ray spectrum with its unique set of peaks, according to energy-dispersive X-ray spectroscopy (EDX). To determine what chemicals composition are in nanospheres, EDX studies were employed. Peaks for Cu and O were discovered, but no peaks for impurities, suggesting that CuO had been clean for a long period (Fig. 5) [36].

3.2. Batch experiments

3.2.1. Effect of pH

The findings regarding the impact of pH show that this factor controls the adsorption process and influences the level of ionization of contaminants, the adsorbent surface charge, and other factors. As depicted in Fig. 6, the obvious from the results of ceftriaxone rises as the initial pH of the solution rises from 2 to 9. When the pH is increased to 12, the removal effectiveness falls down, with the highest removal being shown at a pH of 7. Another explanation for the greater breakdown of CEF in aqueous environments (6.5–7.5) is the restricted hydrolytic effects of alkaline pH. On the other hand, deprotonation and protonation affect the charge of the

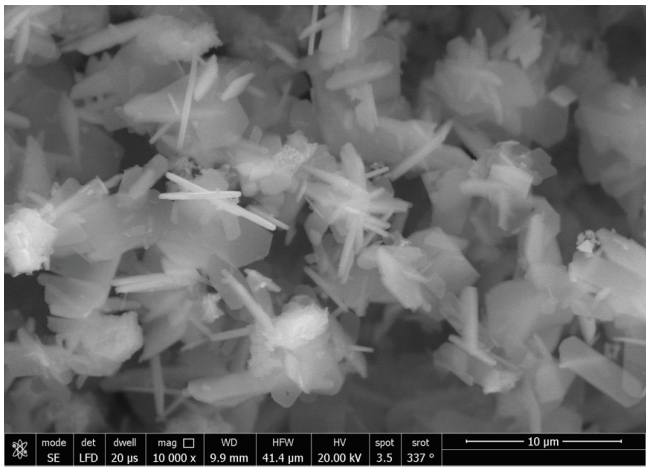

Fig. 4. CuO nanosphere as seen with a scanning electron microscope.

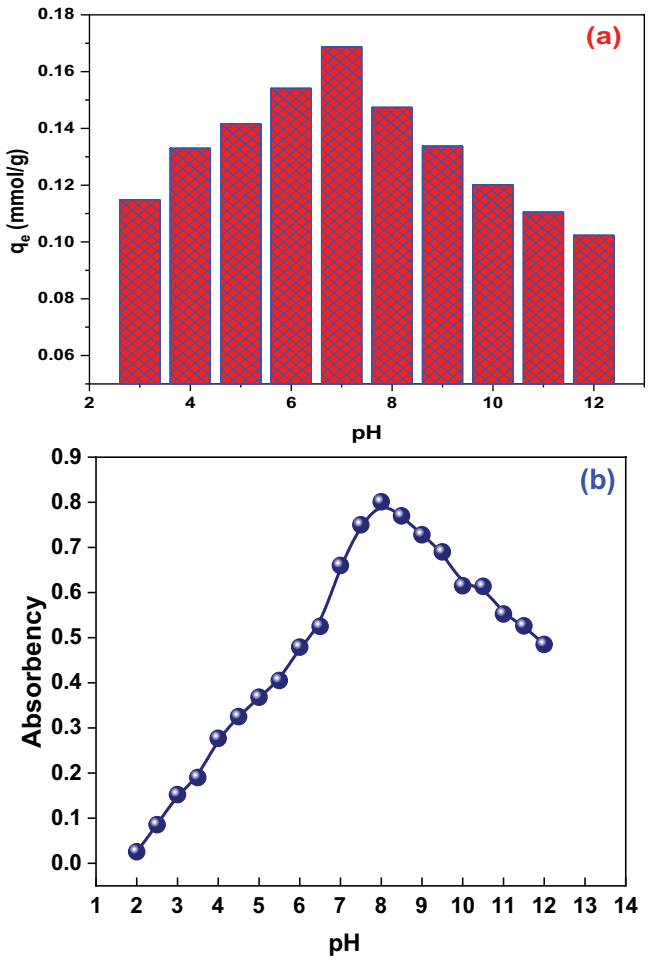

Fig. 6. (a) Employing the adsorbent (CuO) at 450°C, the impact of pH on CEF adsorption. (b) Zeta potential of CuO.

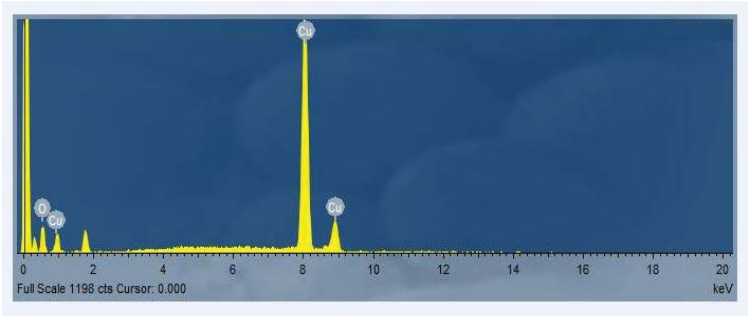

Fig. 5. EDX spectrum of CuO nanosphere.

functional groups in CuO, which has an impact on how well ceftriaxone ions are adsorbed and eliminated. Additionally, the outcomes demonstrate that the binding of ceftriaxone ions to CuO nanospheres is predominantly brought on by the active adsorption sites, primarily Cu and O, in their proton-free form. The weakly acidic molecules that make up CEF have pKa values of 3, 3.2, and 4.1 and an early neutral pH of about 6.7.

In contrast, understanding the adsorption behavior of CEF on CuO nanoparticles depends on the analysis of the electrophoretic behavior by determining the zeta potential. At pH levels under 2, the nanoparticles' surface zeta potential is at its lowest (Fig. 6b); therefore, the attraction force between nanoparticles is stronger than the electrostatic repulsion force between them. As pH increases, the electrostatic repulsion force between nanoparticles becomes strong enough to avoid attraction and collisions caused by Brownian motion because the nanoparticles' surface's zeta potential has increased. With a rise in pH, the absorbency also increases, this improves the CuO nanoparticles' stability during scattering. CuO zeta potential and absorbency increase with a pH of 8, respectively. The scattering stability of CuO nanoparticles is optimal because the coagulated nanoparticles can be mechanically redistributed because the electrostatic repulsion force between the particles is stronger. As the pH value rises, more of the reagent used to regulate pH, NaOH, is present in the system. It causes the electrical double layer to collapse, resulting in a decrease in the electrostatic repulsion force and the zeta potential of the nanoparticles' surface as well as a worse dispersion through nano-suspensions.

3.2.2. Effects of calcination

Investigations were done to determine how CEF adsorption tests will be affected by CuO calcination temperatures of 450°C, 550°C, and 650°C. CuO dose was 0.02 g, and dye solution volume was 25 mL; and concentration was 1.2×10^{-3} mol/L, the pH level was 7, and the shake velocity was 200 rpm. The effectiveness of CuO adsorption increased when the calcination temp was dropped 0.22 > 0.189 > 0.1467 mmol/g for CuO at calcination temperature 450°C, 550°C and 650°C, respectively (Fig. 7) [38,39].

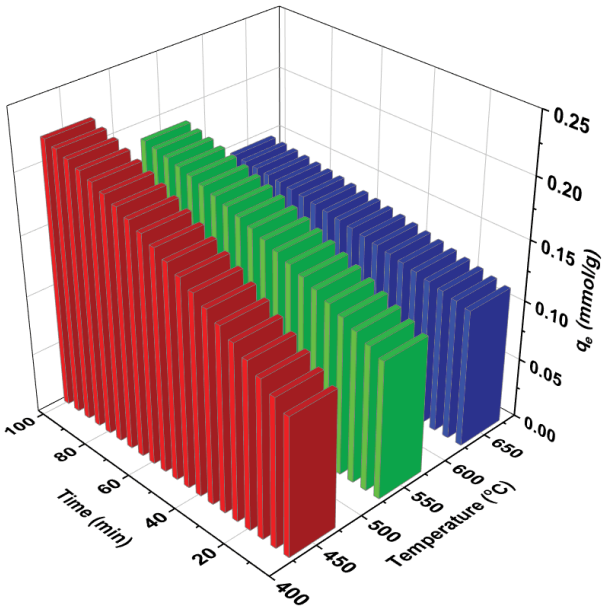

Fig. 7. Influence of CuO calcination temperature on CEF adsorption.

3.2.3. Influence of CuO dosage

As the adsorbent dose (0.01–0.25 g) per 25 mL is changed, the CEF concentration of 2.51×10^{-3} mol/L at 25°C, and pH 7, we looked into the CEF adsorption on sorbent made of CuO nanospheres (Fig. 8). It demonstrates the CEF's capacity to bind to various adsorbent concentrations [40]. As the CuO dose is raised from 0.01 to 0.1 g per 25 mL, the adsorption potential of CEF decreases from 0.13 to 0.05 mmol/g and rises. As the dose rises, the adsorbent's surface area increases and the equilibrium concentration of CEF falls [41].

3.2.4. Adsorption isotherms

Langmuir:

$$\frac{C_e}{q_e} = \frac{1}{q_m K_L} + \frac{C_e}{q_m} \tag{4}$$

Freundlich:

$$\ln q_e = \ln K_F + \frac{1}{n} \ln C_e \tag{5}$$

Dubinin–Radushkevich

$$\ln q_e = \ln Q_{DR} - K_{DR} \varepsilon^2 \tag{6}$$

Temkin

$$q_e = \beta_T \ln K_T + \beta_T \ln C_e \tag{7}$$

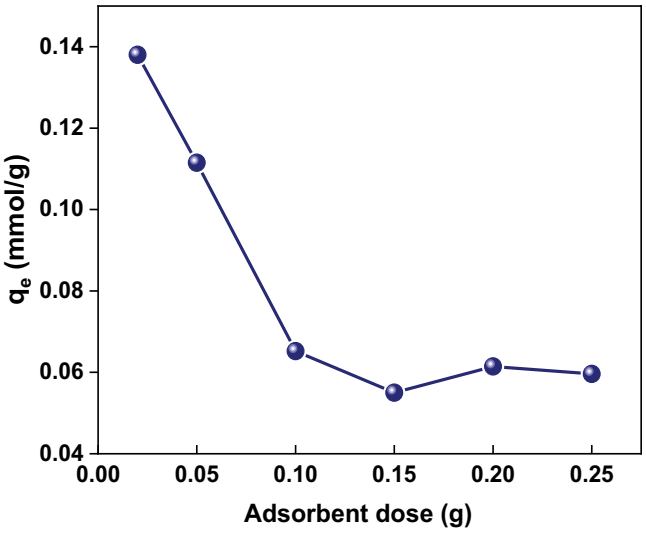

Fig. 8. Influence of CuO dose on CEF adsorption.

CEF absorption on CuO was computed utilizing isotherm models such as Langmuir [42], Freundlich [43], Temkin [44], Dubinin–Radushkevich [45]. Best fit was picked based on the R^2 about one. The isotherm modelling outcomes are outlined in (Table 2). The best fit was found using the Langmuir isotherm model (Fig. 9). This suggests that a monolayer adsorption mechanism is active. The monolayer adsorption potential was 0.25 mmol/g (q_m) and 14.43 kJ/mol is the average value for sorption energy. In respect to the chemisorption process that has been suggested, this is accurate. Indeed, the limit energy for separation is generally agreed to be 8 kJ/mol. Below this value the reaction physisorption and over this value the reaction is chemisorption processes [32,46].

Every time, the fitting coefficients complied with the pattern $R_L^2 > R_T^2 > R_D^2 > R_F^2$, the Langmuir model was found to be most appropriate. In other words, the adsorption mostly occurred on a single layer [49]. In the Freundlich model, the parameter n is temperature-dependent, $1/n$ is the anisotropic factor. If $0 < 1/n < 1$ this mean that favor the removal of the CEF; while if $1/n = 1$ demonstrates that there was no interaction between the adsorbate and the adsorbate throughout the adsorption mechanism; and $1/n > 1$ this indicates the adsorption is difficult. Table 2 demonstrates the outcomes, which demonstrate that the adsorption occurred without any problems, Temkin's isotherm assumes a linear drop in adsorption heat and takes into account adsorbate–adsorbent interactions. The Temkin constants, b_T was 70,285.73 L/mol and A_T was 12.569 kJ/mol, It is confirmed that the adsorption process is physio-chemical in nature. Temkin's isotherm did not fit the data that was gathered and analyzed based on R^2 values [34]. It is possible to use Langmuir and Freundlich in both homogeneous and heterogeneous systems. Table 2 demonstrates that the CEF adsorption process onto CuO nanosphere complies with the Langmuir isotherm.

3.2.5. Adsorption kinetics and mechanism studies

Uptake CEF onto CuO was modeled using the pseudo-first-order [50], pseudo-second-order [51], intraparticle diffusion [51], and Elovich kinetic models in this study [52]. To determine the best fit, the coefficient of determination (R^2) value was used. A diffusion model based on intraparticle mass transfer was used because the pseudo-first-order and pseudo-second-order models were unable to define the governing diffusion mechanisms [53].

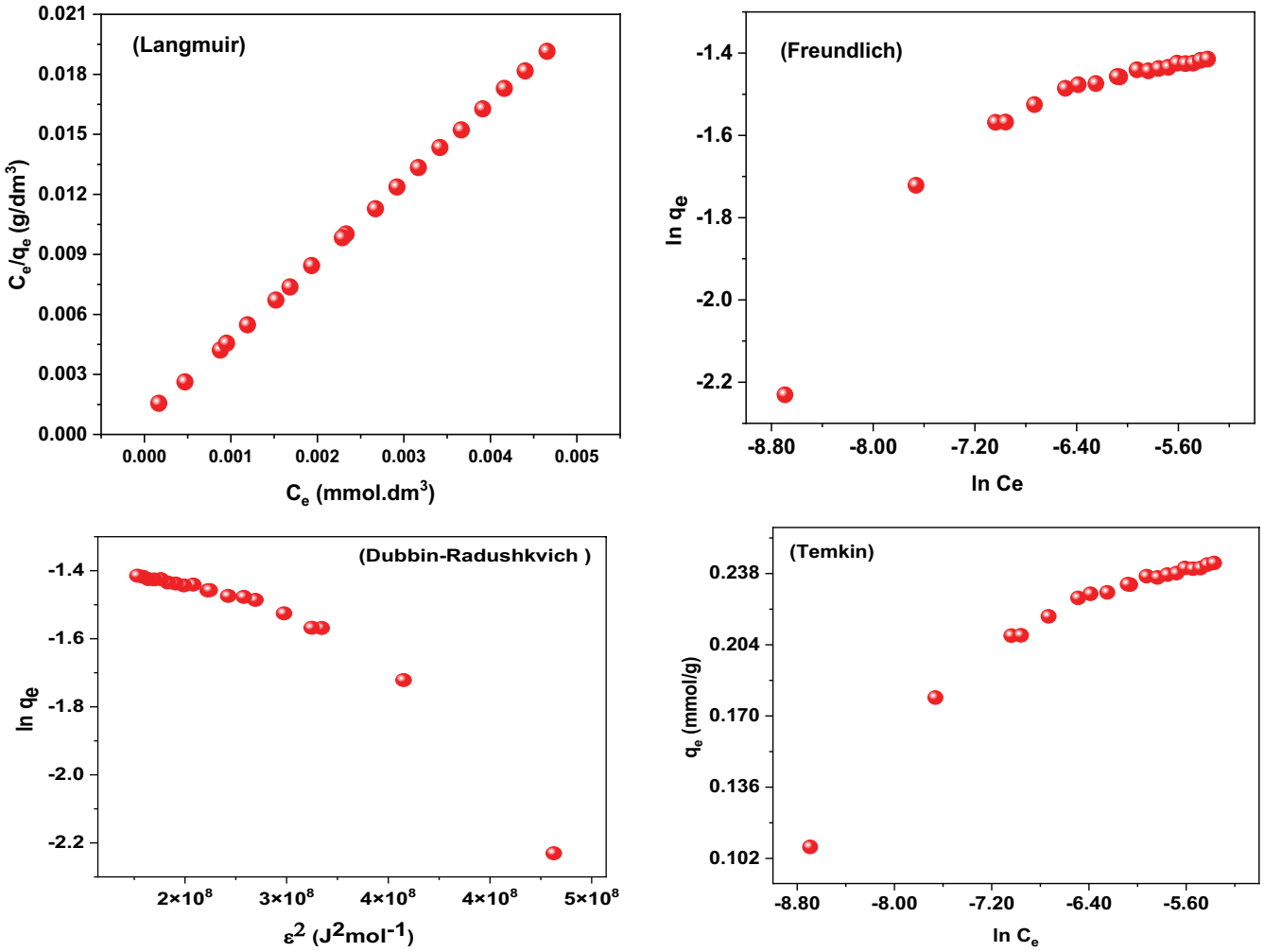

Fig. 9. Linearized isothermal sorption plots for CEF.

Table 2
Isotherms and their linear forms for the adsorption of CEF onto CuO nanosphere [47,48]

Isotherm	Value of parameters	
Langmuir	$q_{m,\exp}$ (mmol/g)	0.245
	q_m (mmol/g)	0.25
	K_L (L/mmol)	5,046.103
	R^2	0.999
Freundlich	n	5.042
	K_F (mmol/g)(L/mmol)$^{1/n}$	0.759
	R^2	0.7737
Dubinin–Radushkevich	Q_{DR}	–0.919
	K_{DR} (J^2/mol^2)	–2.4E-09
	E_a (kJ/mol)	14.43
	R^2	0.864
Temkin	b_T (L/mol)	70,285.73
	A_T (kJ/mol)	12.569
	R^2	0.88

Table 3
Adsorption of CEF onto CuO nanosphere: kinetic parameters and correlation coefficients [47,48]

Model	Value of parameters	
Pseudo-first-order kinetic	K_1 (min^{-1})	0.014
	q_e (mmol/g)	0.13
	R^2	0.898
Pseudo-second-order kinetic	K_2 (g/mg·min)	0.2727
	q_e (mmol/g)	0.244
	R^2	0.984
Intraparticle diffusion	K_i (mg/g·min$^{1/2}$)	–0.0008
	X (mg/g)	0.0109
	R^2	0.979
Elovich	β (g/mg)	–50.352
	α (mg/g·min)	1.08
	R^2	0.40296
Experimental data	q_e (exp) (mmol/g)	0.23

Pseudo-first-order model:

$$\log\left(q_e - q_t\right) = \log q_e - \left(\frac{K_1}{2.303}\right)t \tag{8}$$

Pseudo-second-order:

$$\frac{t}{q_t} = \frac{1}{K_2 q_e^2} + \frac{t}{q_e} \tag{9}$$

Intraparticle diffusion:

$$q_t = K_i t^{1/2} + X \tag{10}$$

Elovich:

$$q_t = \frac{1}{\beta}\ln\left(\alpha\beta\right) + \frac{1}{\beta}\ln t \tag{11}$$

Table 3 summarizes the findings of the kinetics modeling and displays the intraparticle difusion equilibrium constant (K), pseudo-first-order constants (K_1), and pseudo-second-order constants (K_2). Due to its properties, for the adsorption mechanism, the pseudo-second-order is the ideal fit R^2 equals 0.984 is comparatively a greater correlation coefficient (R^2). Designates in the kinetics of absorption, the accessibility of binding sites as well as the quantity of dye in liquid are important considerations. In order to determine the intraparticle diffusion kinetic modelling (R^2 = 0.979) for CEF, the slope of the second-linear region, which equals in (Fig. 10). Early in the process of adsorption, the external barrier to mass transfer around the particles is crucial (initial sharp rise). The 2nd equation portion Intraparticle diffusion technique for continuous adsorption. If the plots not intersect at beginning, This demonstrates that porosity dispersion not only rate-limiting stage; Extra simulations can control the adsorption rate as well, which are both capable of working in tandem [32,54]. As the adsorption sites of CuO heterogeneous, Elovich equation suggests a wide variety of activation energies for chemisorption. Parameter α (associated to the proportion of chemisorption) as the amount of dye in the solution increases, the parameter (which was proportional to the coverage surface) reduced (Table 3), This is because the useful adsorption surface of the adsorbate has decreased [55]. Like a consequence, the speed of chemisorption can be accelerated by increasing the concentration inside the range studied. The excellent accuracy of the pseudo-second-order kinetic model makes it useful for simulating adsorption kinetics. It is predicated on the notion that the frequency step is electrostatic chemisorption, because the adsorbent and the adsorbate share or exchange electrons [56].

3.2.6. Studies of thermodynamic modelling

The change in free energy (ΔG°), enthalpy (ΔH°), and entropy (ΔS°) computed using thermodynamics modeling to investigate several characteristics of CuO's adsorptive elimination of CEF. Table 4 provides an overview of the results of thermodynamic modelling at various temperatures. As (ΔG°) is negatively, the process is both possible and randomized (Fig. 11). (ΔG°) values fell from –0.96 to –4.7 kJ/mol at elevated temperature. As a result, the removal of CEF from CuO becomes more appealing. Plotting (ΔG°) against (T) reveals that it is linear (Fig. 15). (ΔH°), and (ΔS°) 42.97 and 0.149 kJ/mol, respectively, were determined. The presence of positive ΔH° values indicates that the adsorption mechanism is endothermic. A positive value of (ΔS°) identifies the randomness and suggests that the CuO adsorbent has a strong affinity for CEF [47].

$$\ln K_C = -\frac{\Delta H^\circ}{RT} + \frac{\Delta S^\circ}{R} \tag{12}$$

$$\Delta G^\circ = \Delta H^\circ - T\Delta S^\circ \tag{13}$$

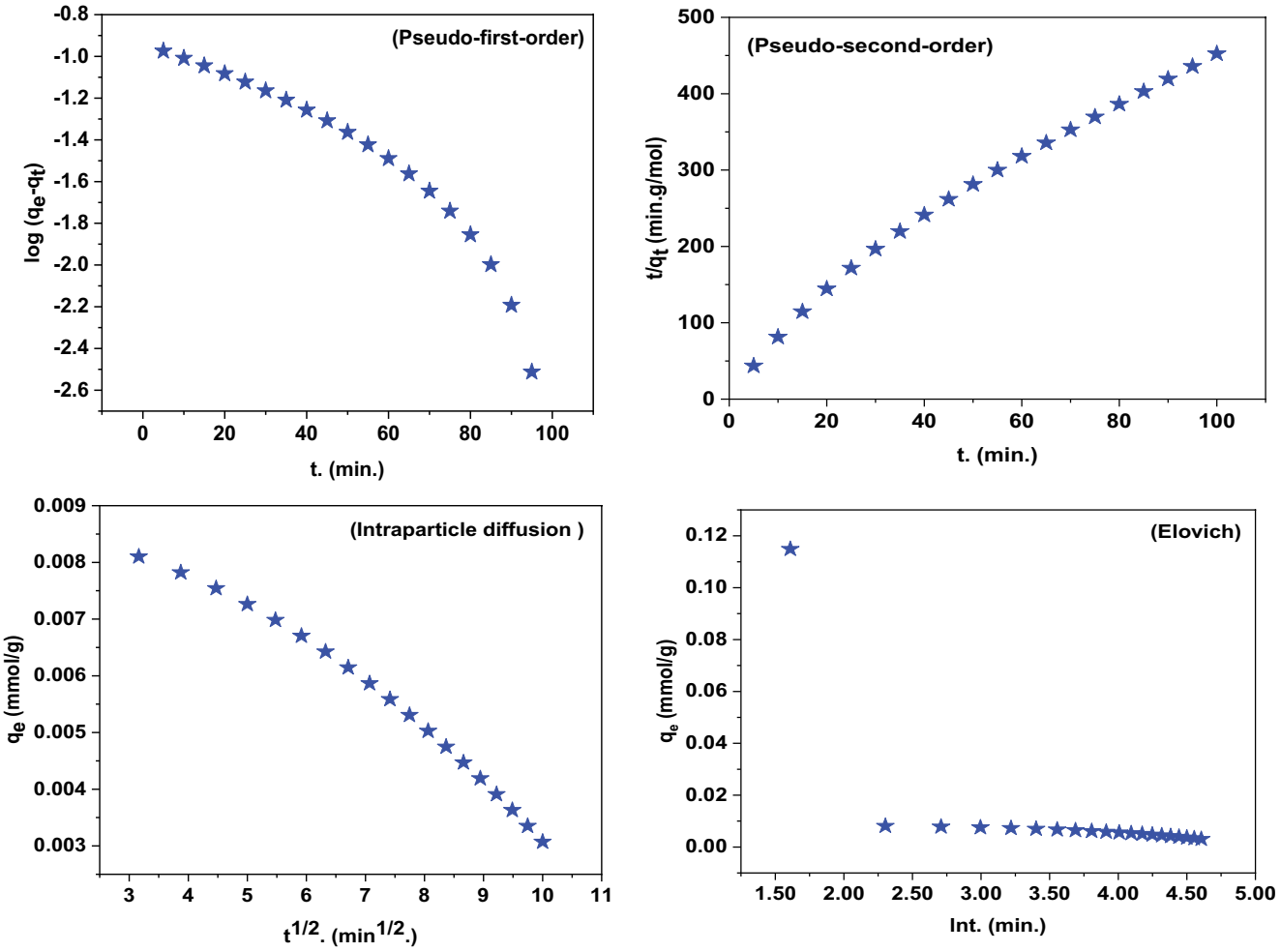

Fig. 10. Linearized isothermal sorption plots for CEF.

Table 4
ΔG°, ΔH°, and ΔS° for TC adsorption on NiO

Drug	T (K)	ΔH° (kJ/mol)	ΔS° (J/mol·K)	T_0 (K)	−ΔG° (kJ/mol)
	298				1.72
	303				2.46
CEF	308	42.97	149.967	286	3.21
	313				3.97
	318				4.70

where is K_C a distribution constant, which is calculated from q_e/C_e, R is a universal constant (8.314 J/mol·K) and T (K) is the adsorption temperature.

The adsorption cycle's slope and intercept were calculated using the lnK_C vs. 1/T plot's. standard (ΔH°) and (ΔS°) was determined. Arrhenius plot intercept was used to compute E_a (Fig. 12). The amount of ΔH° in adsorption processes is positive, indicating an endothermic reaction. While (ΔG°) negatively, it designates spontaneous reaction (Table 4) [54]. In this scenario, the zero standard free energy temperature (T_0) is calculated to be 223 K for CEF. The low T_0 values show that the tested adsorbents are functional and can absorb CEF at very low temperatures.

3.2.7. Active sites

The method of analyzing the adsorption groups the electrophilic/nucleophilic attacking region and the electrostatic potential zero zones in the investigated CEF/CuO systems is referred to as molecular electrostatic potential (MEP). In this study, utilizing molecular electrostatic potentials, the entire electron density surface of CEF was charted (MEP) (Fig. 13) [57].

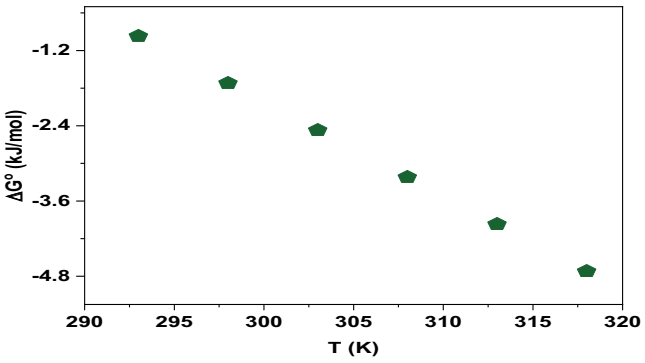

Fig. 11. Graph displays how Gibbs free energy (Δ*G*°) varies with temperature.

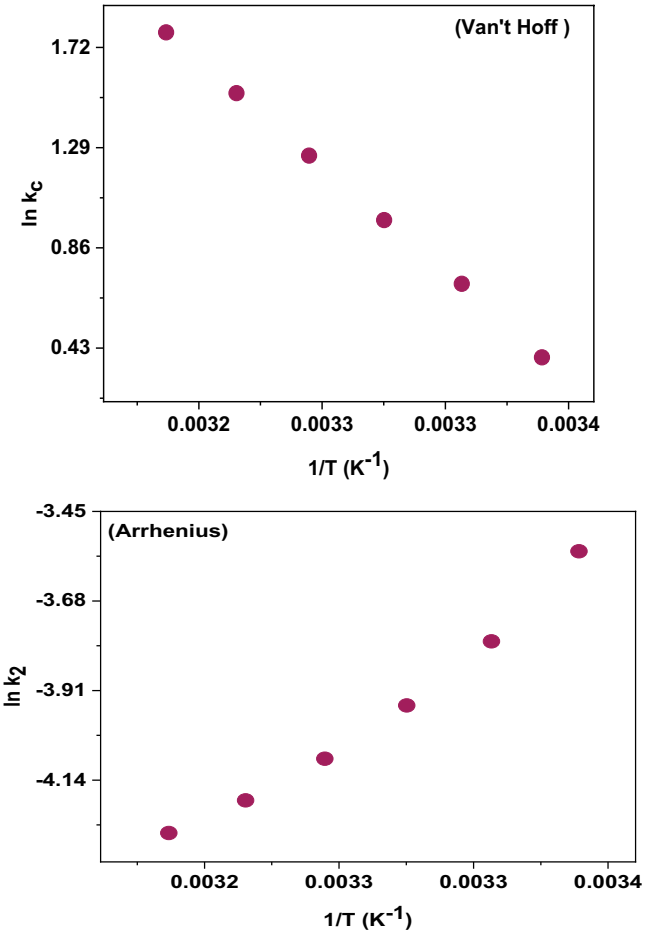

Fig. 12. Thermodynamic adsorption models of CEF onto CuO at 450°C.

On the other hand, have known active binding sites. As a result, if these groups are present, they will boost CEF adsorption, yet the adsorption findings revealed the following: CuO adsorbent capacity in regards of CEF adsorption capacities is owing to that contact in between delocalized electrons in CuO planes and unbound electrons in aromatic rings or many bonds in CEF molecules.

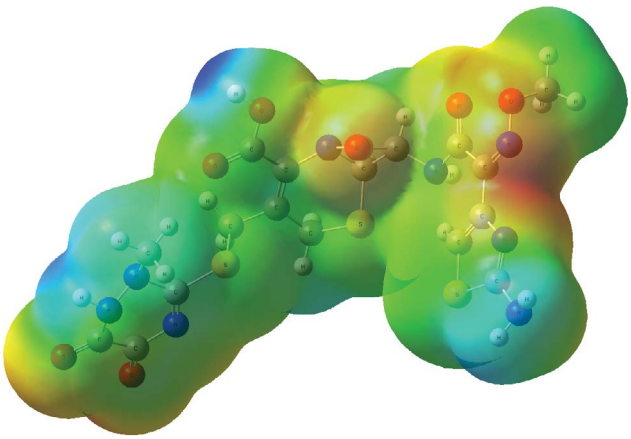

Fig. 13. Molecular electrostatic potential (MEP) for CEF.

Table 5
Examined CEF had its quantum chemical properties determined

Comp.	CEF
E_{HOMO}, eV	–0.227
E_{LUMO}, eV	–0.122
Δ*E*, eV	0.105
X, eV	0.175
η, eV	0.05
Pi, eV	–0.17
σ, eV^{-1}	5.73
S, eV^{-1}	0.026
Ω, eV	0.007
ΔN_{max}	3.32

Table 5 shows the E_{HOMO} and E_{LUMO} principles, and the energy disparity between all compounds, $E_{LUMO-HOMO}$. The difference in energy can be used to find out how hard molecules are and how soft they are (Fig. 14), due to the molecule's lower energy. It is more polarizable and less powerful (more reactive). CEF quantum chemical descriptions were identified as chemical potential (μ), electronegativity (χ), global softness (ϱ), global hardness (η) and electronegativity (χ), global hardness (ϱ), global index of electrophilicity (ω) [41,42].

Indeed, theoretically, the E_{gap} defined as a major reactivity of chemicals component of CEF, a tiny gap denotes a high level of chemical reactivity (poor stable), A huge gap, on the other hand, suggests low chemical reactivity (highly stable) (Table 5).

3.3. Molecular docking

3.3.1. Anti-Candida albicans

In this investigation, the protein database's entry for *Candida albicans* main protease was deleted (1ZAP). Candida was identified in the protein database, however (1ZAP). The most popular method for determining a ligand's binding is to use binding energies [58]. Therefore, a reduction

in binding energy brought on by mutations would improve the ligand's ability to adhere to the receptor [59]. One characteristic that sets ligands apart is the presence of several open active hydrogen bonding sites Fig. 15. They can effectively bind proteins thanks to this feature, which also helps produce inhibitory compounds. Table 6 shows the results that represented a *Candida albicans* mutant 1ZAP-hormone inhibitor is effective.

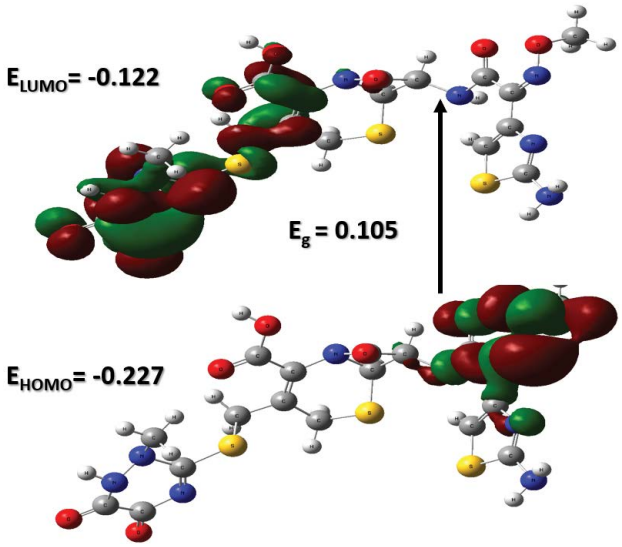

Fig. 14. CEF optimized structures' molecular orbital density distribution at the frontier.

3.3.2. *Heliobacter pylori*

Fig. 16 represented the binding affinity of the CEF towards *Heliobacter pylori* 6gbg-protein while, Table 6 represented the binding energy and amino acids that bind with CEF.

4. Reusability of the CuO for CEF removal

A condition is considered cost-effective when an adsorbent may be used repeatedly while keeping its efficiency for CEF removal, separation, and recovery after regeneration. The separation of CEF that collected by the CuO adsorbent was examined following elution with 0.1-M HCl solution. Any porous substance, including CuO, should be reusable for practical use. We observed a change in CuO's adsorption capacity after three adsorption–desorption cycles. Changing the pH is the most typical approach for desorption of CEF. Desorption is often conducted in uncomplicated environments. By meticulously rinsing 0.02 g of the sorbent in a flask with 0.1 M HCl several times till the pH of the washing solution approached 7, the investigated sorbent CuO was restored. Then, distilled

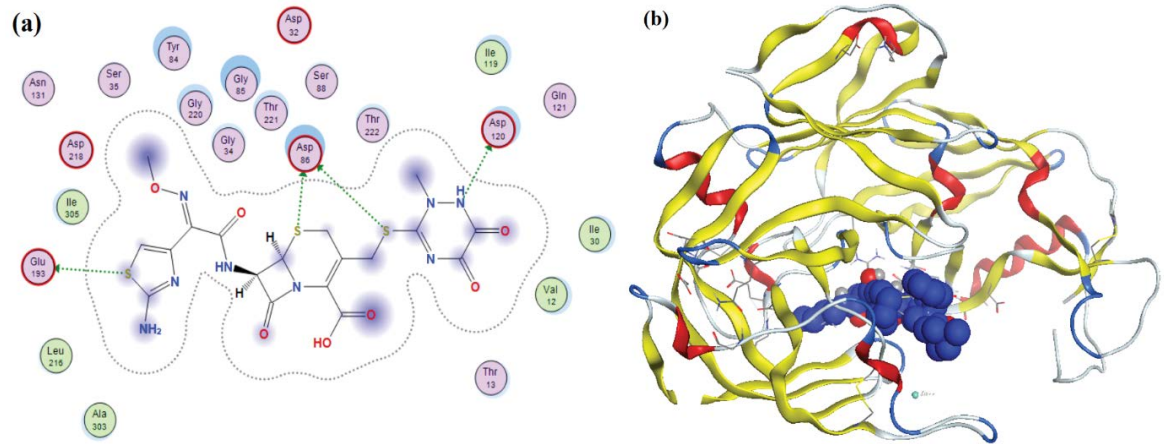

Fig. 15. Molecular docking mode and interaction for the CEF. With *Candida albicans* 1ZAP (a) 2D structure of interaction and (b) 3D structure.

Table 6
Binding interaction between CEF with 1ZAP and 6gbg

Protein	Receptor	Interaction	*E* (kcal/mol)
Candida albicans (1ZAP)	ASP 120	π–π interaction	–7.17
	GLU 193	π–π interaction	
	ASP 86	π–π interaction	
	ASP 86	π–π interaction	
Helicobacter pylori (6gbg)	Gln 408	Hydrogen bond	–6.07
	Gln 405	Hydrogen bond	
	Asn 62	Hydrogen bond	

water was used to clean the adsorbent numerous times. The CuO's remaining colours were taken out using ethanol. After being collected, the clean CuO was roasted for 4 h at 60°C. After being regenerated, the adsorbent was used in the subsequent dye adsorption test. Table 7 displays the outcomes of six cycles of testing the adsorption, desorption, and re-adsorption cycles. They continued by stating that the desorbing medium they used effectively removed the CEF@CuO contact from its surface with a desorptive effectiveness of 98.5%. After then, it was gradually decreased until the sixth cycle, when it was 91.2%. It was obvious that the reason for this slight decrease in the DE % (7.3%) was due to dye molecules aggregating and blocking active areas on the adsorbent surface (chemical reaction). It's also important to note that the CuO's great repeatability was what made water and wastewater treatment systems economically viable. This might be caused by CuO adsorption sites being blocked. The CuO material was also characterised by XRD after undergoing a six-cycle test, and it was discovered that the crystallinity and structure were preserved (Fig. 17). This finding demonstrates the CuO nanospheres' excellent reusability properties.

The regeneration efficacy was calculated using Eq. (14) given:

$$\text{Regeneration efficiency}(\%) = \frac{\text{Quantity of desorbed CEF}}{\text{Amount of CEF absorbed}(\text{mmol})} \times 100 \quad (14)$$

5. Influence of ionic strength

The impact of ionic strength on CuO nanosphere efficiency against CEF was thoroughly simulated in order to evaluate the performance of CuO nanosphere in actual treating wastewater. Purified of CEF is significantly influenced by the quantity of other competing (co-interfering) ions in the aqueous solution, according to Fig. 18. CuO loading capacity has slightly decreased, while the competitor's density has increased (i.e., Cl^-), the adsorption capabilities of the adsorbent for CEF are still remarkable at 0.21 mmol/g (R% = 87.5%). From a wide perspective, the little discrepancy can be discussed as follows. The conflict between disrupted CEF molecules and the CuO nanosphere's adsorbent surface between negatively charged anionic ions (Cl^-) is getting worse. Additionally, protecting the CuO nanosphere surface and slowing the adsorption mechanism were achieved by raising the electrolyte counter ion concentration.

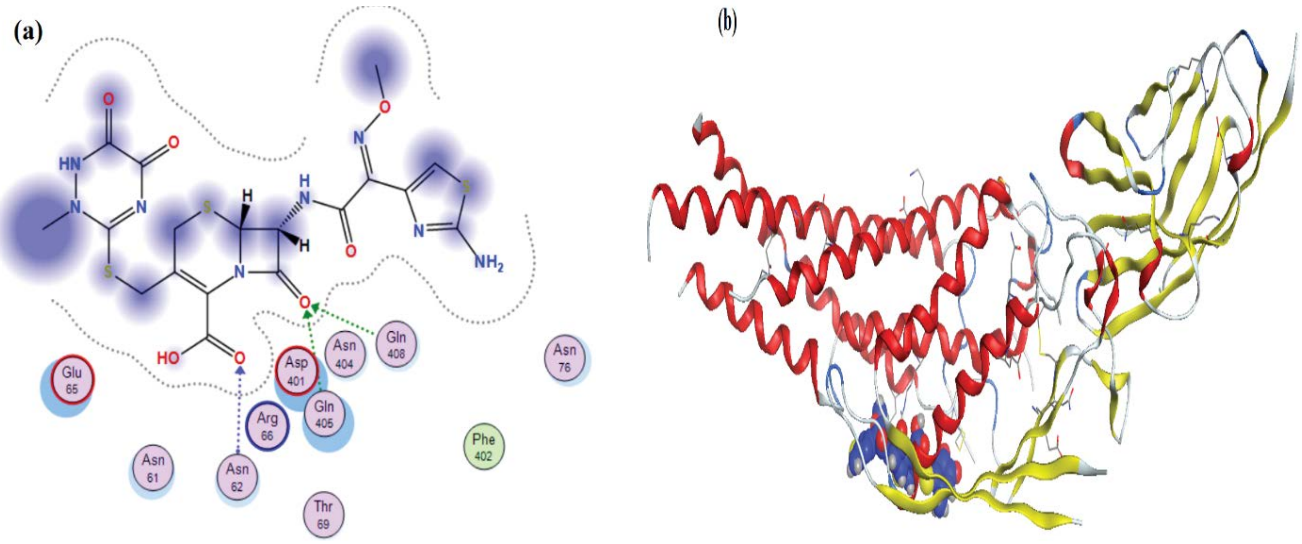

Fig. 16. Molecular docking mode and interaction for the CEF. With *Helicobacter pylori* 6gbg-protein (a) 2D structure of interaction and (b) 3D structure.

Table 7
Adsorption, desorption, and re-adsorption of CEF onto the CuO after six cycles

Adsorption/desorption cycle	q_e (adsorption) (mmol/g)	q_e (desorption) (mmol/g)	Des. (%)
Cycle 1	0.244	0.242	98.5
Cycle 2	0.242	0.238	97.8
Cycle 3	0.238	0.226	96.2
Cycle 4	0.226	0.218	94.3
Cycle 5	0.218	0.21	93.2
Cycle 6	0.21	0.192	91.2

Additionally, the double electric layer contracted with rising solution salinity, creating a repulsive force between the CEF and the adsorbent surface. A more accurate interpretation of Fig. 18 is that several research have discovered that inorganic competitors have inhibitory effects on CEF adsorption employing a variety of adsorbents.

6. Conclusions

CuO was successfully synthesized with calcination of organometallic chelate at 450°C, 550°C and 650°C and made comparison between three samples of obtained copper oxides and found that the best one was 450°C in adsorption of CEF. The mesoporous CuO, which has an adsorption capacity of 127.56 mg/g, could be employed as effective CEF adsorbents. The pseudo-second-order model and the Langmuir model, respectively, were used to characterize the adsorption application's kinetics and isotherm. The ability to separate and regenerate the CuO adsorbents suggests that the CuO nanosphere may be a useful reusable adsorbent for cleaning up CEF pollutants.

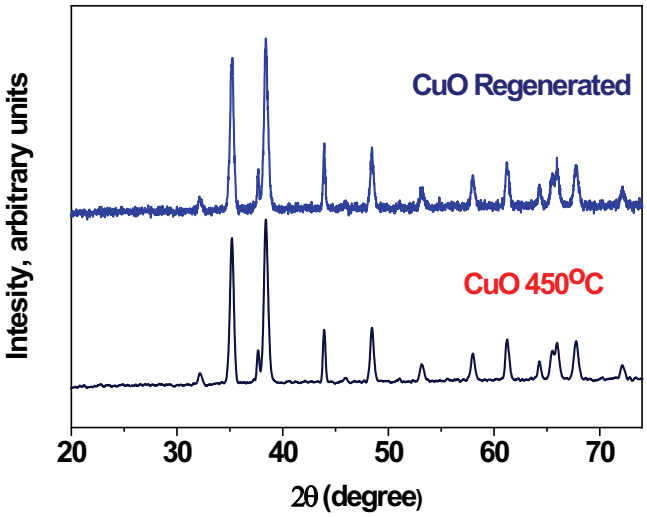

Fig. 17. CuO nanosphere X-ray diffraction spectra at 450°C and regenerate CuO.

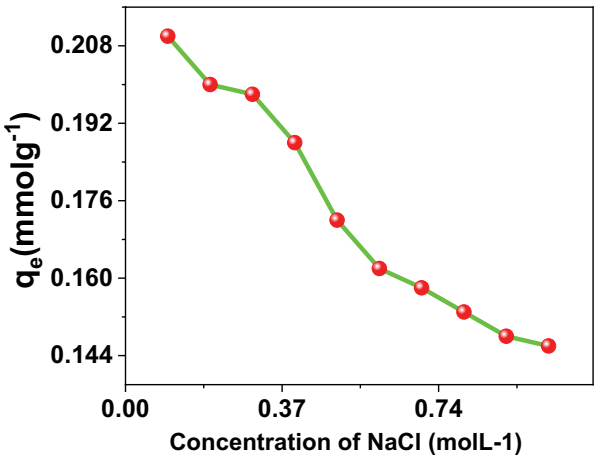

Fig. 18. Influence of ionic strength.

Acknowledgment

This work was supported by Taif University Researchers Supporting Project number (TURSP-2020/2), Taif University, Taif, Saudi Arabia.

References

[1] M. Hoseini, G.H. Safari, H. Kamani, J. Jaafari, M. Ghanbarain, A.H. Mahvi, Sonocatalytic degradation of tetracycline antibiotic in aqueous solution by sonocatalysis, Toxicol. Environ. Chem., 95 (2013) 1680–1689.

[2] S. Bozorginia, J. Jaafari, K. Taghavi, S.D. Ashrafi, E. Roohbakhsh, D. Naghipour, Biosorption of ceftriaxone antibiotic by *Pseudomonas putida* from aqueous solutions, Int. J. Environ. Anal. Chem., (2021) 1–15, doi: 10.1080/03067319.2021.1887858.

[3] J. Jaafari, A.B. Javid, H. Barzanouni, A. Younesi, N. Amir, A. Farahani, M. Mousazadeh, P. Soleimani, Performance of modified one-stage Phoredox reactor with hydraulic up-flow in biological removal of phosphorus from municipal wastewater, Desal. Water Treat., 171 (2019) 216–222.

[4] J. Jaafari, K. Yaghmaeian, Response surface methodological approach for optimizing heavy metal biosorption by the blue-green alga *Chroococcus* disperses, Desal. Water Treat., 142 (2019) 225–234.

[5] M. Pirsaheb, T. Khosravi, K. Sharafi, M. Mouradi, Comparing operational cost and performance evaluation of electrodialysis and reverse osmosis systems in nitrate removal from drinking water in Golshahr, Mashhad, Desal. Water Treat., 57 (2016) 5391–5397.

[6] D. Naghipour, L. Hoseinzadeh, K. Taghavi, J. Jaafari, Characterization, kinetic, thermodynamic and isotherm data for diclofenac removal from aqueous solution by activated carbon derived from pine tree, Data Brief, 18 (2018) 1082–1087.

[7] S.M. Mousavi, M. Nasrabadi, Discussion of "remediation of heavy metals contaminated silty clay loam soil by column extraction with ethylenediaminetetraacetic acid and nitrilo triacetic acid" by Dariush Naghipour, Jalil Jaafari, Seyed Davoud Ashrafi, and Amir Hossein Mahvi, J. Environ. Eng., 144 (2018) 07018003, doi: 10.1061/(ASCE)EE.1943-7870.0001375.

[8] J. Jafari, A. Mesdaghinia, R. Nabizadeh, M. Farrokhi, A.H. Mahvi, Investigation of anaerobic fluidized bed reactor/aerobic moving bed bio reactor (AFBR/MMBR) system for treatment of currant wastewater, Iran. J. Public Health, 42 (2013) 860–867.

[9] M. Seyedsalehi, J. Jaafari, C. Hélix-Nielsen, G. Hodaifa, M. Manshouri, S. Ghadimi, H. Hafizi, H. Barzanouni, Evaluation of moving-bed biofilm sequencing batch reactor (MBSBR) in operating A^2O process with emphasis on biological removal of nutrients existing in wastewater, Int. J. Environ. Sci. Technol., 15 (2018) 199–206.

[10] J.P. Bound, N. Voulvoulis, Predicted and measured concentrations for selected pharmaceuticals in UK rivers: implications for risk assessment, Water Res., 40 (2006) 2885–2892.

[11] P. Vasudevan, V. Padmavathy, N. Tewari, S. Dhingra, Biosorption of heavy metal ions, J. Sci. Ind. Res., 60 (2001) 112–120.

[12] M. Kumar, V. Leon, A.D.S. Materano, O.A. Ilzins, I. Galindo-Castro, S.L. Fuenmayor, Polycyclic aromatic hydrocarbon degradation by biosurfactant-producing *Pseudomonas* sp. IR1, Z. Naturforsch., C: Biosci., 61 (2006) 203–212.

[13] D. Naghipour, K. Taghavi, M. Ashournia, J. Jaafari, R. Arjmand Movarrekh, A study of Cr(VI) and NH^{4+} adsorption using greensand (glauconite) as a low-cost adsorbent from aqueous solutions, Water Environ. J., 34 (2020) 45–56.

[14] R. Gupta, P. Ahuja, S. Khan, R. Saxena, H. Mohapatra, Microbial biosorbents: meeting challenges of heavy metal pollution in aqueous solutions, Curr. Sci., 78 (2000) 967–973.

[15] M. Cycoń, A. Mrozik, Z. Piotrowska-Seget, Antibiotics in the soil environment—degradation and their impact on microbial activity and diversity, Front. Microbiol., 10 (2019) 338, doi: 10.3389/fmicb.2019.00338.
[16] M. Jafari, S.F. Aghamiri, G. Khaghanic, Batch adsorption of cephalosporins antibiotics from aqueous solution by means of multi-walled carbon nanotubes, World Appl. Sci. J., 14 (2011) 1642–1650.
[17] M.E. Mahmoud, A.M. El-Ghanam, R.H.A. Mohamed, S.R. Saad, Enhanced adsorption of levofloxacin and ceftriaxone antibiotics from water by assembled composite of nanotitanium oxide/chitosan/nano-bentonite, Mater. Sci. Eng., C, 108 (2020) 110199, doi: 10.1016/j.msec.2019.110199.
[18] A.A. Beni, A. Esmaeili, Y. Behjat, Invent of a simultaneous adsorption and separation process based on dynamic membrane for treatment Zn(II), Ni(II) and, Co(II) industrial wastewater, Arabian J. Chem., 14 (2021) 103231, doi: 10.1016/j.arabjc.2021.103231.
[19] A. Esmaeili, S. Shirzad Nagadehi, Construction and optimization of polyethylene membrane with polyamides to remove pollutants and investigate their efficiency solar system, Int. J. Environ. Sci. Technol., 17 (2020) 3691–3704.
[20] A.A. Beni, A. Esmaeili, Biosorption, an efficient method for removing heavy metals from industrial effluents: a review, Environ. Technol. Innovation, 17 (2020) 100503, doi: 10.1016/j.eti.2019.100503.
[21] A.A. Beni, A. Esmaeili, Design and optimization of a new reactor based on biofilm-ceramic for industrial wastewater treatment, Environ. Pollut., 255 (2019) 113298, doi: 10.1016/j.envpol.2019.113298.
[22] A. Esmaeili, B. Saremnia, Comparison study of adsorption and nanofiltration methods for removal of total petroleum hydrocarbons from oil-field wastewater, J. Pet. Sci. Eng., 171 (2018) 403–413.
[23] M.G. El-Desouky, M.A. Khalil, A.A. El-Bindary, M.A. ElBindary, Biological, biochemical and thermochemical techniques for biofuel production: an updated review, Biointerface Res. Appl. Chem., 12 (2022) 3034–3054.
[24] G.A.A. AlHazmi, Kh.S. AbouMelha, M.G. El-Desouky, A.A. El-Bindary, Effective adsorption of doxorubicin hydrochloride on zirconium metal-organic framework: equilibrium, kinetic and thermodynamic studies, J. Mol. Struct., 1258 (2022) 132679, doi: 10.1016/j.molstruc.2022.132679.
[25] T.J. Al-Musawi, A.H. Mahvi, A.D. Khatibi, D. Balarak, Effective adsorption of ciprofloxacin antibiotic using powdered activated carbon magnetized by iron(III) oxide magnetic nanoparticles, J. Porous Mater., 28 (2021) 835–852.
[26] D. Balarak, N. Mengelizadeh, P. Rajiv, K. Chandrika, Photocatalytic degradation of amoxicillin from aqueous solutions by titanium dioxide nanoparticles loaded on graphene oxide, Environ. Sci. Pollut. Res., 28 (2021) 49743–49754.
[27] A.A. El-Bindary, M.G. El-Desouky, M.A.M. El-Afify, Thermal and spectroscopic studies of some prepared metal complexes and investigation of their potential anticancer and antiviral drug activity against SARS-CoV-2 by molecular docking simulation, Biointerface Res. Appl. Chem., 12 (2021) 1053–1075.
[28] M. Yilmaz, T.J. Al-Musawi, A.D. Khatibi, M. Baniasadi, D. Balarak, Synthesis of activated carbon from *Lemna minor* plant and magnetized with iron(III) oxide magnetic nanoparticles and its application in removal of ciprofloxacin, Biomass Convers. Biorefin., (2022) 1–14, doi: 10.1007/s13399-021-02279-y.
[29] M.G. El-Desouky, A. Shahat, A.A. El-Bindary, M.A. El-Bindary, Description, kinetic and equilibrium studies of the adsorption of carbon dioxide in mesoporous iron oxide nanospheres, Biointerface Res. Appl. Chem., 12 (2021) 3034–3054.
[30] MG. El-Desouky, AA. El-Bindary, MAM. El-Afify, N. Hassan, Synthesis, characterization, theoretical calculation, DNA binding, molecular docking, anticovid-19 and anticancer chelation studies of some transition metal complexes, Inorg. Nano-Metal Chem., 52 (2022) 1–16.
[31] N. Hassan, A. El-Sonbati, M. El-Desouky, Synthesis, characterization, molecular docking and DNA binding studies of Cu(II), Ni(II), Zn(II) and Mn(II) complexes, J. Mol. Liq., 242 (2017) 293–307.
[32] M.G. El-Desouky, A.A. El-Bindary, Magnetic metal-organic framework (Fe_3O_4@ZIF-8) nanocomposites for adsorption of anionic dyes from wastewater, Inorg. Nano-Metal Chem., (2021) 1–15, doi: 10.1080/24701556.2021.2007131.
[33] N. Hassan, A. Shahat, A. El-Didamony, M. El-Desouky, A. El-Bindary, Synthesis and characterization of ZnO nanoparticles via zeolitic imidazolate framework-8 and its application for removal of dyes, J. Mol. Struct., 1210 (2020) 128029, doi: 10.1016/j.molstruc.2020.128029.
[34] G.H. Al-Hazmi, M.G. El-Desouky, A.A. El-Bindary, Synthesis, characterization and microstructural evaluation of ZnO nanoparticles by William-Hall and size-strain plot methods, Bull. Chem. Soc. Ethiop., 36 (2022) 815–829.
[35] M.S. Frost, M.J. Dempsey, D.E. Whitehead, The response of citrate functionalised gold and silver nanoparticles to the addition of heavy metal ions, Colloids Surf., A, 518 (2017) 15–24.
[36] A. Fouda, S.S. Salem, A.R. Wassel, M.F. Hamza, T.I. Shaheen, Optimization of green biosynthesized visible light active CuO/ZnO nano-photocatalysts for the degradation of organic methylene blue dye, Heliyon, 6 (2020) e04896, doi: 10.1016/j.heliyon.2020.e04896.
[37] F. Ramezani, R. Zare-Dorabei, Simultaneous ultrasonic-assisted removal of malachite green and methylene blue from aqueous solution by Zr-SBA-15, Polyhedron, 166 (2019) 153–161.
[38] A.S. Al-Wasidi, I.I. AlZahrani, A.M. Naglah, M.G. El-Desouky, M.A. Khalil, A.A. El-Bindary, M.A. El-Bindary, Effective removal of methylene blue from aqueous solution using metal-organic framework; modelling analysis, statistical physics treatment and DFT calculations, ChemistrySelect, 6 (2021) 11431–11447.
[39] M. Saghanejhad Tehrani, R. Zare-Dorabei, Competitive removal of hazardous dyes from aqueous solution by MIL-68(Al): derivative spectrophotometric method and response surface methodology approach, Spectrochim. Acta, Part A, 60 (2016) 8–18.
[40] M.G. El-Desouky, M. Abd El-Wahab, A.A. El-Bindary, Interpretations and DFT calculations for polypropylene/copper oxide nanosphere, Biointerface Res. Appl. Chem., 12 (2021) 1134–1147.
[41] A.A. Mohammadi, A. Zarei, H. Alidadi, M. Afsharnia, M. Shams, Two-dimensional zeolitic imidazolate framework-8 for efficient removal of phosphate from water, process modeling, optimization, kinetic, and isotherm studies, Desal. Water Treat., 129 (2018) 244–254.
[42] I. Langmuir, The adsorption of gases on plane surfaces of glass, mica and platinum, J. Am. Chem. Soc., 40 (1918) 1361–1403.
[43] H. Freundlich, W. Heller, The adsorption of cis-and trans-azobenzene, J. Am. Chem. Soc., 61 (1939) 2228–2230.
[44] M.J. Temkin, V. Pyzhev, Recent modifications to Langmuir isotherms, Acta Physiochim. URSS, 12 (1940) 217–225.
[45] M.M. Dubinin, E. Zaverina, L. Radushkevich, Sorption and structure of active carbons. I. Adsorption of organic vapors, Zh. Fiz. Khim., 21 (1947) 151–162.
[46] T.A. Altalhi, M.M. Ibrahim, G.A.M. Mersal, M.H.H. Mahmoud, T. Kumeria, M.G. El-Desouky, A.A. El-Bindary, M.A. El-Bindary, Adsorption of doxorubicin hydrochloride onto thermally treated green adsorbent: equilibrium, kinetic and thermodynamic studies, J. Mol. Struct., 1263 (2022) 133160, doi: 10.1016/j.molstruc.2022.133160.
[47] M. El-Desouky, M. El-Bindary, A. El-Bindary, Effective adsorptive removal of anionic dyes from aqueous solution, Vietnam J. Chem., 59 (2021) 341–361.
[48] M.A. El-Bindary, M.G. El-Desouky, A.A. El-Bindary, Adsorption of industrial dye from aqueous solutions onto thermally treated green adsorbent: a complete batch system evaluation, J. Mol. Liq., 346 (2021) 117082, doi: 10.1016/j.molliq.2021.117082.
[49] G.A.A. Al-Hazmi, M.A. El-Bindary, M.G. El-Desouky, A.A. El-Bindary, Efficient adsorptive removal of industrial dye from aqueous solution by synthesized zeolitic imidazolate framework-8 loaded date seed activated carbon and statistical physics modeling, Desal. Water Treat., 258 (2022) 85–103.

[50] S.K. Lagergren, About the theory of so-called adsorption of soluble substances, Sven. Vetenskapsakad. Handingarl, 24 (1898) 1–39.
[51] Y.-S. Ho, G. McKay, Sorption of dye from aqueous solution by peat, Chem. Eng. J., 70 (1998) 115–124.
[52] G.A.A. Al-Hazmi, A.A. El-Zahhar, M.G. El-Desouky, M.A. El-Bindary, A.A. El-Bindary, Efficiency of Fe_3O_4@ZIF-8 for the removal of doxorubicin from aqueous solutions: equilibrium, kinetics and thermodynamic studies, Environ. Technol., (2022) 1–48, doi: 10.1080/09593330.2022.2121181.
[53] D. Karataş, D. Senol-Arslan, O. Ozdemir, Experimental and atomic modeling of the adsorption of acid azo dye 57 to sepiolite, Clays Clay Miner., 66 (2018) 426–437.
[54] G. Mohamed, A. Ashraf, A. Mohamed, Low-temperature adsorption study of carbon dioxide on porous magnetite nanospheres iron oxide, Biointerface Res. Appl. Chem., 12 (2021) 6252–6268.
[55] G. Mohamed, N. Hassan, A. Shahat, A. El-Didamony, A. Ashraf, Synthesis and characterization of porous magnetite nanosphere iron oxide as a novel adsorbent of anionic dyes removal from aqueous solution, Biointerface Res. Appl. Chem., 11 (2021) 13377–13401.
[56] N.C. Corda, M.S. Kini, A review on adsorption of cationic dyes using activated carbon, MATEC Web Conf., 144 (2018) 02022, doi: 10.1051/matecconf/201814402022.
[57] A.S. Al-Wasidi, I.I.S. AlZahrani, H.I. Thawibaraka, A.M. Naglah, M.G. El-Desouky, M.A. El-Bindary, Adsorption studies of carbon dioxide and anionic dye on green adsorbent, J. Mol. Struct., 1250 (2021) 131736, doi: 10.1016/j.molstruc.2021.131736.
[58] C. Huang, Y. Wang, X. Li, L. Ren, J. Zhao, Y. Hu, L. Zhang, G. Fan, J. Xu, X. Gu, Clinical features of patients infected with 2019 novel coronavirus in Wuhan, China, The LANCET, 395 (2020) 497–506.
[59] P. Gautret, J.-C. Lagier, P. Parola, V.T. Hoang, L. Meddeb, M. Mailhe, B. Doudier, J. Courjon, V. Giordanengo, V.E. Vieira, H. Tissot Dupont, S. Honoré, Philippe, Hydroxychloroquine and azithromycin as a treatment of COVID-19: results of an open-label non-randomized clinical trial, Int. J. Antimicrob. Agents, 56 (2020) 105949, doi: 10.1016/j.ijantimicag.2020.105949.

Supporting information

S1. Materials and methods

S1.1. Materials and apparatus

Spectroscopic level was obtained from Sigma-Aldrich (Germany), Fluka (India) and Merck from all the reagents and solvents.

S2.2. Characterization of CuO

Fourier-transform infrared spectroscopy (FTIR) were measured in a Nicolet iS10 system. Samples were grinded with KBr for FTIR measurements in the wave number range of 4,000–400 cm^{-1}. The powder X-ray diffraction forms were plotted using PANalytical X'Pert Pro instrument using iron-filtered Cu-Kα radiation (λ = 1.5406 Å) in the 2θ from 5° to 50° with a step size of 0.02° and at a time scan of 0.3 s. UV-Vis-DRS spectra were recorded by using HACH LANGE GmbH, Germany UV-Vis spectrophotometer. N_2 adsorption and desorption isotherms were measured at the boiling temperature of liquid nitrogen (–196°C) on ASAP 2020 (Micromeritics, USA). The sample were prepared by exposed to vacuum (5×10^{-3} torr) at 200°C in order to ensure a clean surface. Using Brunauer–Emmett–Teller method, from which the Barrett–Joyner–Halenda pore volume and Brunauer–Emmett–Teller surface area and were measured. Scanning electron microscopy images with energy-dispersive X-ray spectroscopy (EDX) were resulted with a ZEISS SEM with tungsten filament as electron source operated at 10–20 kV. EDX spectra and elemental mapping were recorded using Oxford Instruments X-Max system and INCA analysis software diffuse.